Neuropeptides 73 (2019) 78–88

Contents lists available at ScienceDirect

Neuropeptides

journal homepage: www.elsevier.com/locate/npep

Skeletal phenotype of the neuropeptide Y knockout mouse☆

Natalie K.Y. Wee[a], Benjamin P. Sinder[a], Sanja Novak[a], Xi Wang[a], Chris Stoddard[b], Brya G. Matthews[a,c], Ivo Kalajzic[a,*]

[a] Department of Reconstructive Sciences, Farmington, CT 06030, USA
[b] Genetics and Genome Sciences, UConn Health, Farmington, CT 06030, USA
[c] Department of Molecular Medicine and Pathology, University of Auckland, Auckland 1023, New Zealand

ARTICLE INFO

Keywords:
Neuropeptide Y (NPY)
Conditional mouse
Bone
Cortical bone
Bone strength

ABSTRACT

Neuropeptide Y (NPY) is involved in multiple processes such as behavior, energy and bone metabolism. Previous studies have relied on global NPY depletion to examine its effects on bone. However, this approach is unable to distinguish the central or local source of NPY influencing bone. Our aim was to identify which cells within the skeleton express *Npy* and establish a model that will enable us to differentiate effects of NPY derived from different cell types. We have generated the NPY floxed (NPY^{flox}) mice using CRISPR technology. By crossing the NPY^{flox} mice with Hypoxanthine Phosphoribosyltransferase 1 (*Hprt*)-cre to generate a global knockout, we were able to validate and confirm loss of *Npy* transcript and protein in our global NPYKO.

Global deletion of NPY results in a smaller femoral cortical cross-sectional area (−12%) and reduced bone strength (−18%) in male mice. *In vitro*, NPY-deficient bone marrow stromal cells (BMSCs) showed increase in osteogenic differentiation detected by increases in alkaline phosphatase staining and bone sialoprotein and osteocalcin expression. Despite both sexes presenting with increased adiposity, female mice had no alterations in bone mass, suggesting that NPY may have sex-specific effects on bone. In this study we identified *Npy* expression in the skeleton and examined the effect of global NPY depletion to bone mass. The differential impact of NPY deletion in cortical and cancellous compartments along with differences in phenotypes between *in vitro* and *in vivo*, highlights the complex nature of NPY signaling, indicative of distinct sources that can be dissected in the future using this NPY^{flox} model.

1. Introduction

Over the past two decades, our knowledge of the interactions between bone and the nervous system has expanded. Following the discovery of hypothalamic regulation of bone mass, recent studies have focused on local regulation of the osteoblast and osteoclast lineage by neuropeptides (Ducy et al., 2000; Baldock et al., 2002; Matic et al., 2012; Lee et al., 2011, 2015; Horsnell and Baldock, 2016). Neuropeptide Y (NPY) is a 36 amino acid hydrophilic peptide that is highly abundant in the central and peripheral nervous systems (Schwartz et al., 1990; Blomqvist and Herzog, 1997). It is an orexigenic peptide that regulates metabolic processes through the hypothalamus, but also, has a role in peripheral tissues. NPY signaling is involved in a number of processes such as behavior, energy homeostasis, immune function and bone metabolism (Blomqvist and Herzog, 1997; Wee et al., 2016; Wheway et al., 2007; Karl et al., 2008). In addition to the nervous system, neuropeptides are expressed in peripheral tissues including bone and various cell types localized to the bone marrow environment (Igwe et al., 2009; Paic et al., 2009; Alves et al., 2016).

NPY signaling is known to influence the skeleton (Baldock et al., 2002, 2007, 2009; Matic et al., 2012; Igwe et al., 2009). NPY and its related peptides peptide YY (PYY) and pancreatic peptide (PP) signal through a family of 5 receptors known as Y receptors (Y1, Y2, Y4, Y5, y6). Hypothalamic regulation of bone is exerted by both Y1 and Y2 receptors and through the effects by peripheral sympathetic nervous system (Baldock et al., 2002, 2007, 2014). Deletion of Y1 and Y2 receptors in the brain revealed that NPY signaling inhibits osteogenesis (Baldock et al., 2002, 2007). In addition, global deletion of NPY resulted in increased osteoblastic activity (Baldock et al., 2009). Interestingly, addition of NPY to the hypothalamic area in NPY global knockout mice resulted in only a partial rescue of the bone phenotype (Baldock et al., 2009). This indicated a potential role of peripheral

☆ Supported by: This work has been supported by NIH/NIAMS grants AR055607, AR066218, Connecticut Innovations (CI) 16-RMB-UCHC-10 and REP funds to I.K, and Health Research Council of New Zealand Sir Charles Hercus Fellowship to BGM.

* Corresponding author
E-mail address: ikalaj@uchc.edu (I. Kalajzic).

https://doi.org/10.1016/j.npep.2018.11.009
Received 9 August 2018; Received in revised form 4 November 2018; Accepted 28 November 2018
Available online 30 November 2018
0143-4179/

sources of NPY as regulators of bone mass. As osteoblast lineage cells express NPY Y1 receptor, global deletion and bone directed deletion of Y1 targeting mature (Col2.3Cre) and early (Col3.6Cre) osteoblasts resulted in increased bone mass (Lee et al., 2010, 2011).

To date, the source of NPY responsible for the activation of Y1 receptors on osteoblast lineage cells has not been defined. Besides *Npy* expression by sympathetic nerves in periosteum and bone marrow (Tabarowski et al., 1996), our lab has previously demonstrated that *Npy* expression is highly enriched in osteocytes, in comparison to pre-osteoblasts, osteoprogenitors and osteoblasts (Paic et al., 2009). Previous studies have relied on global deletion of NPY to examine its effects on the skeleton (Baldock et al., 2009; Park et al., 2016; Wang et al., 2016; Wee et al., 2018), but there is a clear need to develop inducible cell type targeted conditional knockout mice for better definition of cell source and mechanisms of action of NPY. The aim of this study was to develop and characterize the NPY conditional knockout (NPYKO) mouse, which will facilitate cell-specific depletion of NPY.

2. Materials and methods

2.1. Mouse strains and colony management

All procedures were approved by the UConn Health Institutional Animal Care and Use Committee and performed in an AAALAC accredited facility. Mice were group housed in ventilated cages with a 12 h light cycle (7 am-7 pm). The room temperature was maintained at 22 °C. Water and irradiated rodent chow (Teklad 2918, Invigo, Indianapolis, IN) was provided *ad libitum*.

2.1.1. Generation of the NPY conditional knockout construct

Vectors pl452 and pl451 were designed with targeting arms to place a loxp site (pl452) upstream of the exon1 and frt-loxP site (pl451) downstream of exon 2. Clustered Regularly Interspaced Short Palindromic Repeats (CRISPR) vectors using px330 were designed to cut in the locations to which the vectors would be targeted. A CRISPR plasmid was co-electroporated with the upstream targeting vector into mouse embryonic stem cells and were selected with G418. Colonies were picked and screened by polymerase chain reaction (PCR) for correct targeting. Positive clones were transfected with a CreIRESpuro for transient expression of Cre and cultured with puromycin for 2 days. Surviving clones were analyzed for complete recombination of the pl452 cassette leaving behind the upstream loxP. These clones were then co-electroporated with a CRISPR designed to cut downstream of the second exon along with a targeting vector to target a frt-neofrt-loxP cassette. Clones were selected with G418, picked, and analyzed. The analysis was to both identify clones with targeting as well as clones with the targeting on the same allele as the upstream loxp site. Positive embryonic stem cell (ES) clones were aggregated with morula and transferred to recipient females. Pups were bred with a FLP mouse to recombine the frt-neofrt-loxp leaving behind the downstream loxP site creating the floxed NPY mouse as represented in Fig. 1A. These NPY^{flox} mice were backcrossed on a C57BL/6 J background for 8 generations.

2.1.2. Generation of NPY global knockout mice

Male NPY^{flox} mice were bred with female Hypoxanthine Phosphoribosyltransferase 1 (*Hprt*)-cre mice (129S1/Sv-*Hprttm1(CAG-cre)Mnn*/J that were backcrossed > 10 generations on a C57/Bl6 background) to remove the floxed *Npy* gene in the embryo generating global knockout (Fig. 1B). Upon confirmation of NPY deletion, this line was maintained by crossing heterozygous mice, to generate all three genotypes – wildtype (WT), heterozygous and knockout (NPYKO). Littermate WT and NPYKO mice were assessed for a phenotype.

2.2. RNA extraction and real time PCR

RNA was extracted from bone marrow stromal cell (BMSC) cultures using Trizol (Ambion, Foster City, CA) according to the manufacturer's protocol and quantified using a Nanodrop One (Thermofisher, Waltham, MA). Depending on the RNA yield obtained, samples were screened for integrity either by loading 0.5μg into a 1.5% agarose gel and visualized using ethidium bromide or loaded onto an Experion Eukaryote Total RNA HighSensitivity chip (BioRad, Hercules, CA). RNA samples were DNAse treated (DNAse I, Cat. # 18068015, Invitrogen, Carlsbad, CA) and cDNA was synthesized using Improm-II Reverse Transcription kit (Cat. # A3800, Promega, Madison, WI). qPCR was run using the following Taqman (Applied Biosystems, Waltam, MA) probes: *Npy* (Mm03048253_m1), *Y1* (Mm00650798_g1), *Bsp* (Mm00492555_m1) and *Ocn* (Mm03413826_mH). Genes were normalized to housekeeping gene *Gapdh* (Mm99999915_g1). Relative expression of target genes was calculated using the ΔΔCt method.

2.3. Genotyping for the NPYfloxed allele and NPY deletion

DNA was extracted from tail tissue. Genotyping was performed using the specified primers as listed in Table 1 with the following run conditions: 95 °C for 3 mins, 34 cycles (95 °C for 30 s, 58.7 °C for 30 s, 72 °C for 30 s), followed by 72 °C for 3 mins. The products were subsequently loaded into a 2% agarose gel in Tris-acetate-EDTA (TAE) buffer and run for 40 min at 100 V. The PCR product was stained with ethidium bromide and visualized using a ChemiDoc imaging system (BioRad) (Fig. 1C).

2.4. Immunohistochemistry

Brain samples were fixed in 4% paraformaldehyde (PFA) for 3 days, and then 30% sucrose at 4 °C, prior to cryo-embedding. Tissues were cut at 7 μm thickness on Cryotape (Cryofilm 2C, Section Lab, Japan) and cross-linked using Norland Optical Adhesive 61 (Norland Optical, Cranbury, NJ) onto glass slides. Sections were permeabilized with 0.3% Triton, peroxide treated (3% hydrogen peroxide), blocked with 5% rabbit serum, incubated with 1:5000 dilution of NPY antibody (Cat#:22940; Immunostar, Hudson, WI), 1:80 dilution of biotinylated secondary antibody and the rest of the staining was completed using the Vector peroxidase substrate kit DAB (Cat#: SK-4100; Vector Laboratories, Burlingame, CA). Sections were counter-stained with haematoxylin. Sections were mounted in 50% glycerol and imaged using a Zeiss Observer Z.1 microscope with an AxioCam MRc camera and Zen Pro 2012 software.

2.5. Tissue collection

To evaluate dynamic histomorphometry, mice were injected with calcein (10 mg/kg Sigma-Aldrich, St. Louis, MO) nine days and alizarin complexone (30 mg/kg Sigma-Aldrich, St. Louis, MO) two days before they were euthanized at 14 weeks of age. The right femur was fixed in PFA and stored in phosphate-buffered saline (PBS) for microCT, then transferred to 30% sucrose and frozen at −20 °C prior to cryo-embedding. The left femur was wrapped in PBS-soaked gauze and was frozen at −20 °C until torsion testing. The left gonadal fat pad was dissected-free, weighed and fixed in 4% PFA.

2.6. MicroCT

Femoral morphometry of 14 week-old mice was assessed using conebeam micro-focus X-ray computed tomography (μCT40, Scanco Medical AG, Switzerland). Serial tomographic images were acquired at 55 kV and 145 μA, collecting 1000 projections per rotation at 300 ms integration time. Three-dimensional 16-bit grayscale images were reconstructed using standard convolution back-projection algorithms with Shepp and Logan filtering, and rendered within a 16.4 mm field of view at a discrete density of 244,140 voxels/mm3 (isometric 16 μm voxels). Segmentation of bone was performed in conjunction with a

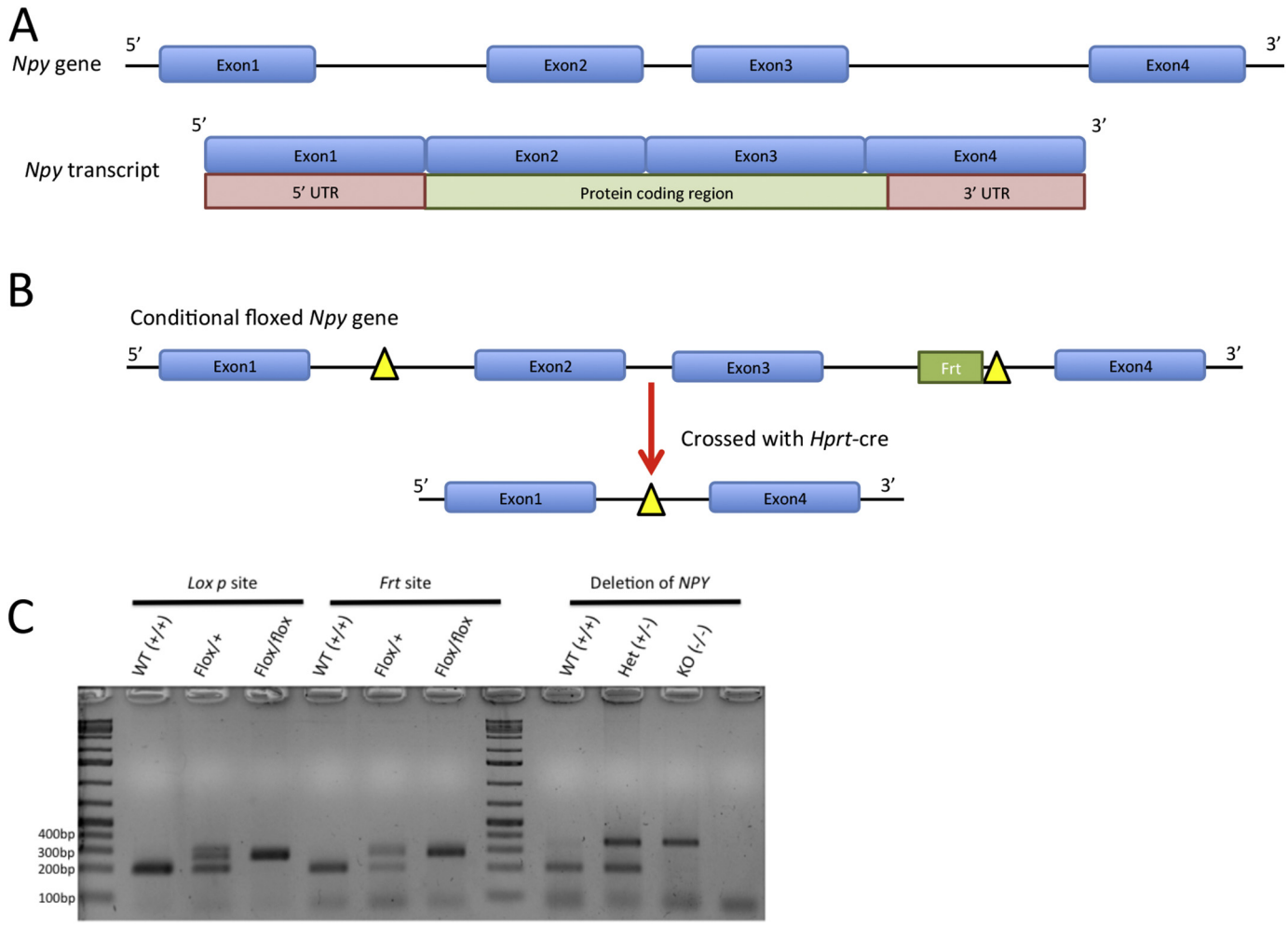

Fig. 1. Generation of NPY^{flox}and global NPYKO. Structure and coding region of the NPY gene (A). Schematic diagram of the NPY^{flox} allele and how the global NPYKO was generated (B). PCR demonstrating the incorporation of the loxP and Frt sites and validate NPY deletion in the global NPYKO (C). Expression was not detectable (ND) by qPCR.

Table 1
PCR sequences for genotyping.

Primer pair	Sequence	Product size
Lox p site		
NPYgtloxpF	GCCTCCGTGCCTCTTATCTT	WT – 204 bp
NPYgtloxpR	GATTTTGGAGGCAACAGAGC	Mut – 270 bp
Frt site		
NPYgtfrtF	CCAATCCTATCGCATCCCTA	WT – 198 bp
NPYgtfrtR	CTATCTGGAGGTGGCAGGTC	Mut – 278 bp
NPY deletion		
NPYgtloxpF	GCCTCCGTGCCTCTTATCTT	WT – 198 bp
NPYgtfrtF	CCAATCCTATCGCATCCCTA	KO – 353 bp
NPYgtfrtR	CTATCTGGAGGTGGCAGGTC	

constrained Gaussian filter to reduce noise, applying calibrated hydroxyapatite-equivalent density thresholds of 495 and 740 mg/cm^3 for trabecular and cortical bone, respectively. Trabecular morphometry was measured in the distal femur metaphysis, defining a volumetric region of interest within the endocortical surface of a 1 mm span referenced 1 mm from the growth plate. Cortical morphometry was measured within a 600 µm span, referenced 5.1 mm from the growth plate.

2.7. Mechanical testing (torsion)

For torsion testing, femurs were potted in methyl methacrylate (Orthodontic Resin, Dentisply Caulk Inc. Milford, DE) bone cement in aluminum jigs, allowed to rehydrate in PBS for one hour at room temperature and tested for biomechanical properties using outward rotation on a TestBench™ Torsion Testing system (Bose Corporation ElectroForce Systems Group, Eden Prairie, MN). Data aquisition rate was 10 Hz, 1 degree/s. Data were plotted as torque to rotation; bone strength (N.mm), stiffness (N.mm/deg) and twist to failure (deg) were determined.

2.8. Histomorphometry of bone

Cryosections (7 µm) from undecalcified femurs were prepared as described above. The calcein/alizarin labels were evaluated under a dual filter using Osteomeasure (Osteometrics, Atlanta, GA). A second set were decalcified with 14% EDTA then stained with tartrate resistant acid phosphatase (TRAP) kit (Cat. #387A, Sigma-Aldrich, St. Louis, MO). TRAP sections were also evaluated using Osteomeasure. Histomorphometric measurements were obtained in a manner consistent with reported guidelines and nomenclature (Dempster et al., 2013).

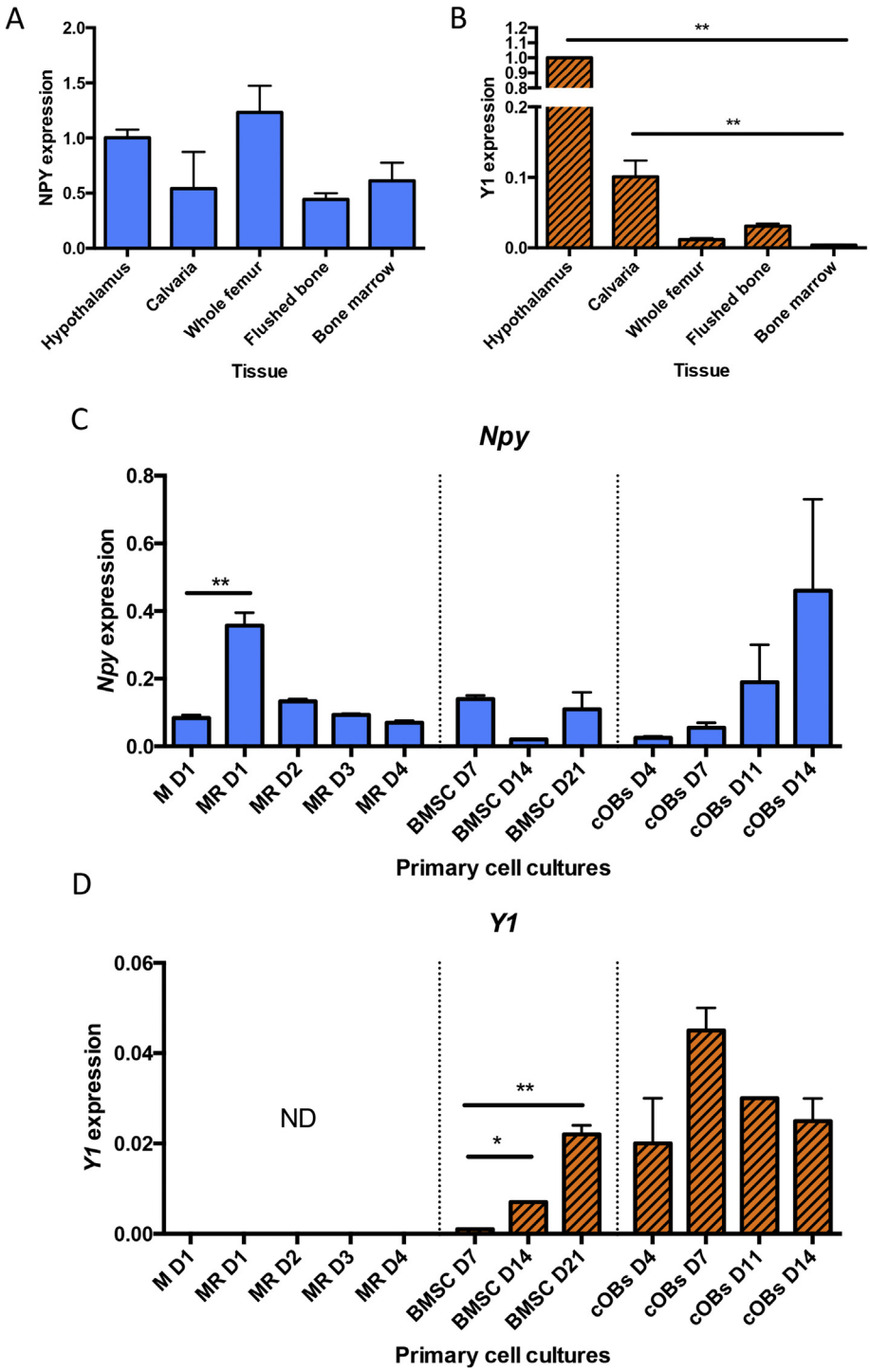

Fig. 2. ***NPY and Y1 are locally expressed in bone tissue.*** NPY (A) and Y1 expression (B) in hypothalamus and bone tissue. NPY (C) and Y1 (D) expression in primary cell cultures of bone marrow monocytes/macrophages (BMMs) stimulated with mCSF only (day 1) and in response to mCSF and RANKL stimulation (M + R; days 1–4), bone marrow stromal cells (BMSCs) undergoing differentiation (days 7, 14, 21) and calvarial osteoblasts (cOB) (day 4, 7, 11, 14). Mean ± SEM. All samples were normalized to hypothalamic levels. Expression was not detectable (ND) by qPCR. Statistical analyses: one-way ANOVA, where $*p < .05$ and $**p < .01$. BMM cultures – $n = 3$; BMSC culture – $n = 2$; calvarial osteoblasts – $n = 2$.

2.9. Whole body DXA

Mice were anaethetised with ketamine/xylaxine cocktail and whole body dual-energy X-ray absorptiometry (DXA) was performed on a Lunar Piximus II (GE, Fitchburg, WI). Each scan was analyzed so that the rectangular region of interest (ROI) began at the ankles of the forelimbs and ended at the ankles of the hind limbs. Both the head and tail were excluded from the ROI. The following measurements were derived from the whole body DXA scans: lean mass, fat mass, % fat mass, bone mineral density (BMD) and bone mineral content (BMC).

2.10. Sectioning of adipose tissue

Following fixation, the gonadal fat pad was dehydrated in an ethanol gradient and then placed into xylene prior to embedding in paraffin. 5 µm sections were cut on a microtome and stained with Mayers haematoxylin (Polyscientific R&D; Bay Shore, NY) and eosin (Shandon Eosin Y alcoholic #6766007; Thermofisher).

2.11. Bone marrow stromal cell (BMSC) cultures

Bone marrow cells were flushed from femora and tibiae from female mice. The cells were plated at a seeding density of 1×10^7 cells per well

in a 6 well plate in alpha minimal essential media (α-MEM) media (Gibco, Billings, MT) supplemented with 10% heat-inactivated fetal bovine serum (FBS) and 5 U Penicillin/Streptomycin (P/S). Osteogenic media consisted of α-MEM, 10% FBS, P/S, 50 μg/mL ascorbic acid and 8 mM β-glycerophosphate. Alkaline leukocyte phosphatase (ALP) staining was performed using ALP staining kit (Cat. #86R, Sigma-Aldrich, St. Louis, MO). The results of the staining were imaged using a scanner, Epson Perfection 1240 (Seiko Epson Corporation, Nagano Japan).

2.12. Calvarial osteoblast cultures

Calvariae were isolated from P5 pups. Parietal bones were digested at 37 °C in 0.05% trypsin and collagenase P (0.5 mg/mL) in PBS for 30 mins at a time; discarding the first fraction and keeping the subsequent 3 fractions. Cells were plated at a density of 2×10^5 cells per well in a 6 well plate and were changed to osteogenic media on Day 7. RNA was extracted on Day 4, 7, 11 and 14 of culture.

2.13. Bone marrow mononuclear cell cultures (BMM)

BMMs were prepared as previously described (Yeon Won et al., 2016). Bone marrow cells were prepared and cultured in α-MEM media with 10% FBS overnight on tissue culture. Non-adherent cells were then layered over the Ficoll Hypaque (GE Healthcare, Piscataway, NJ, USA) and centrifuged to remove red blood cells and stromal cells. Cells were cultured in macrophage-colony stimulating factor (M-CSF) alone or with stimulation by Receptor activator of nuclear factor kappa-B ligand (RANKL) (both at 30 ng/mL; R&D Systems, Minneapolis, MN) for the days indicated with medium change on day 3.

2.14. Statistical analyses

All data were expressed as means ± standard error of the mean (SEM). Differences between groups were assessed by *t*-tests or one-way ANOVAs and followed by *post hoc* Tukey tests, if applicable. The statistical test used for each graph is stated in the figure legend. Statistical analyses were performed using Prism 6 (GraphPad software, CA, USA).

3. Results

3.1. NPY and Y1 expression in bone tissue

We evaluated the presence of *NPY* and *Y1* expression in murine skeletal tissue. Hypothalamic RNA from WT mice was included as a positive control for both probes (Fig. 2A,B). *Npy* expression was detected in calvaria, whole femur, flushed bone (bone with periosteum removed and bone marrow flushed out), and bone marrow at levels similar to what was detected in the hypothalamus (Fig. 2A). *Y1* expression was detected in calvaria, whole femur and flushed bone; we were unable to detect *Y1* expression in bone marrow (Fig. 2B). Interestingly, flushed bone showed an enrichment of *Y1* expression compared to whole femur and bone marrow.

To further investigate *Npy* and *Y1* expression within specific cell types present in bone, we isolated several primary skeletal cell types from WT mice. *Npy* expression was detected in bone marrow monocytes and osteoclast cultures across all times points (Fig. 2C); most notably, initial stimulation with RANKL increased *Npy* expression by 4 fold. Expression of *Npy* was identified in bone marrow stromal cell (BMSC) cultures that were undergoing differentiation with osteogenic media (ascorbic acid and β-glycerophosphate) (Fig. 2C). However, these cultures are heterogeneous in their preparation as they are prepared by culturing flushed bone marrow cells (Chang et al., 2008). Thus, NPY in BMSC cultures is not necessarily arising from BMSCs or osteoblasts *per se*. Increasing levels of *Npy* expression were detected in calvarial osteoblast cultures between day 4 and Day 14 (Fig. 2C). *Y1* receptor expression was not detected in bone marrow mononuclear cells (BMMs) (Fig. 2D). Thus, BMMs may contribute as a source of NPY, but are unable to respond to NPY stimulation. *Y1* expression was found as BMSCs differentiated into osteoblasts and higher Y1 expression was observed in calvarial osteoblast cultures (Fig. 2D). Thus, we were able to demonstrate that NPY is produced in skeletal tissues and cells of the osteoblast lineage express the *Y1* receptor reinforcing the notion that they respond to changes in NPY levels.

3.2. Generation and validation of NPY^{flox} and global NPYKO models

The *Npy* gene in the mouse is located on chromosome 6 and consists of 4 exons. The protein-coding region of the *Npy* transcript is made up of exon 2, exon 3 and the first part of exon 4 (Fig. 1A). The NPY floxed model was generated using CRISPR technology by inserting a loxP site between Exon 1 and Exon 2 and an Frt-loxP site between Exon 3 and Exon 4 to flank all but two protein-coding amino acids (Fig. 1B; for full details, see Materials and Methods). Global NPY deficient mice (NPYKO) were generated by crossing *Hprt*-cre mice with the NPY^{flox} mice (Fig. 1B). The insertion of the loxP site (≈270 bp) and frt site (≈278 bp) for the NPY^{flox} and recombination of the *NPY* locus for the global NPYKO (≈353 bp) were verified by PCR (Fig. 1C). Deletion of exons 2 and 3 in the NPYKO resulted in a loss of *Npy* gene expression in the adrenal gland, brain and bone tissues (Fig. 3A). The highest expression of *Npy* occurs in the arcuate nucleus (Schwartz et al., 1990; Blomqvist and Herzog, 1997). Therefore, we confirmed absence of the protein in the arcuate nucleus of NPYKO mice by immunohistochemistry (Fig. 3B). Thus, we were able to establish the first NPY conditional knockout mouse and generate a global NPY-deficient mouse using our conditional knockout.

3.3. Increased adiposity in male NPY-deficient mice

NPY is implicated in the regulation of whole body energy homeostasis; Y1 deficient mice develop adult-onset obesity at around 12–15 weeks of age (Baldock et al., 2007; Zhang et al., 2010). In our global NPY-deficient model, at 14 weeks of age, no difference in body weight (Fig. 3C) or lean mass (Fig. 3D) was present in male WT and NPYKO mice. An increase in fat mass (Fig. 3E, $p = .07$) and %fat mass (Fig. 3F) was observed in male NPYKO mice. Serum leptin levels were correlated with fat mass (Males $R^2 = 0.64$, $p = .06$; Females: $R^2 = 0.76$, $p < .01$). We identified that our NPY-deficient mice had increased leptin levels compared to WT mice in both genders (Fig. 3G), consistent with the observed increase in fat mass (Fig. 3E,F). The relationship between fat mass and leptin levels was not altered in NPYKO mice, suggesting that in our model NPY deficiency does not directly affect circulating leptin levels. There was also a trend towards increased gonadal fat pad weight in male mice (Fig. 3H, $p = .10$; Fig. 3I, $p = .07$). Increased adipocyte size was observed in the gonadal fat pads of NPYKO mice (Fig. 3J). Altogether, we identified an increase in adiposity in NPYKO mice, suggesting that whole body energy metabolism is altered in this global NPY-deficient model.

3.4. Male NPY-deficient mice have a smaller cross-sectional area and impaired bone strength

Male NPYKO mice had no difference in body weight at 14 weeks of age (Fig. 4A). Femoral length was shorter by 2% in NPYKO mice in comparison to WT (Fig. 4B). We assessed for changes in cortical bone mass using microCT and bone strength using torsion testing. In males, NPYKO mice had significant reductions in total and marrow area by 12% and 15% respectively (Fig. 4C–E). There was a trend towards reduced cortical area in male mice (Fig. 4F, $p = .07$), but no difference in cortical thickness (Fig. 4G). This corresponded with reductions in periosteal and endosteal perimeters in male mice (Fig. 4H, I). Changes in cortical cross-sectional area can impact bone strength (van der

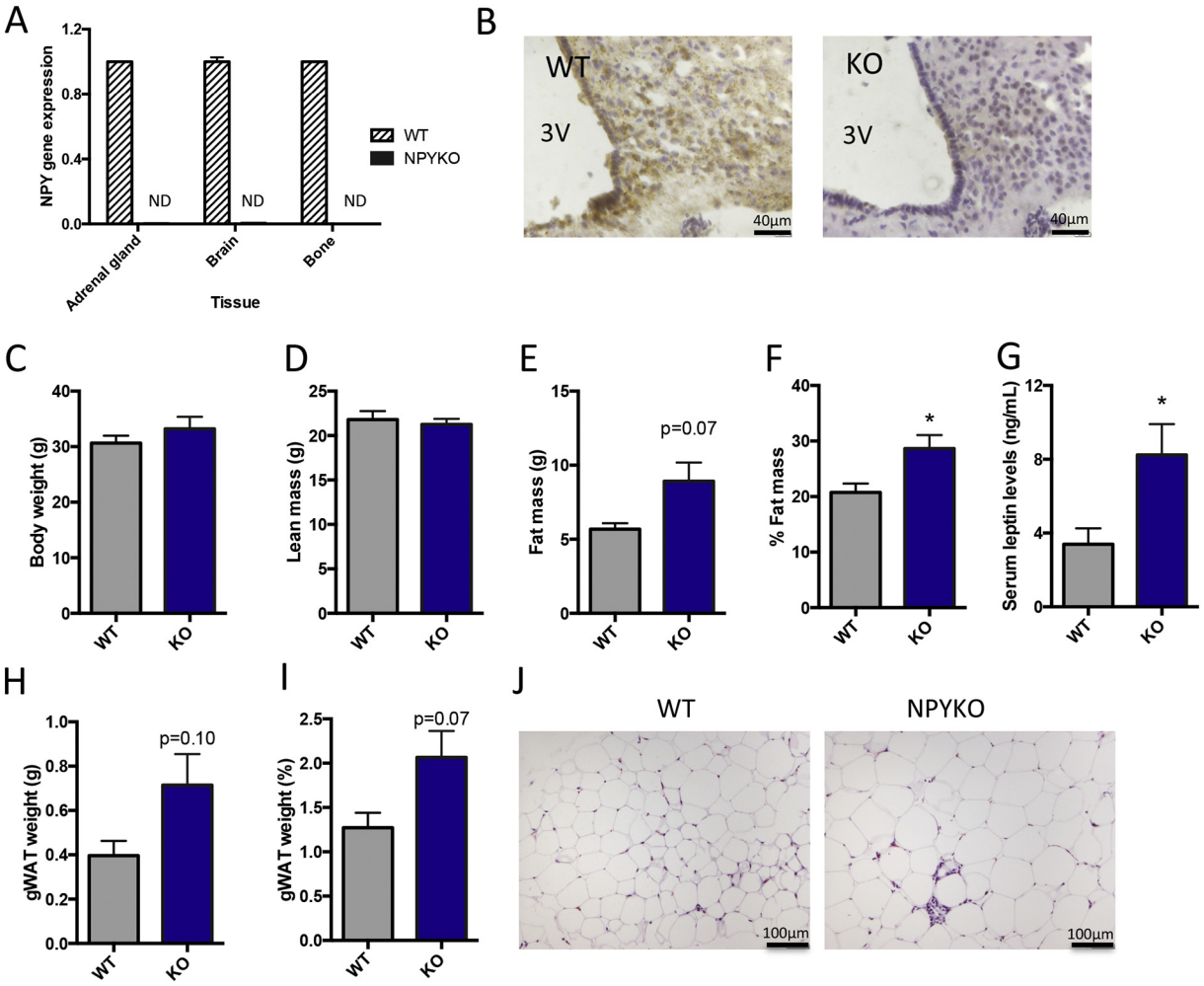

Fig. 3. ***Validation of global NPYKO and evaluation of body composition.*** Gene expression of NPY in adrenal gland, brain and bone (A), $n = 3$. Immunohistochemistry for NPY in arcuate nucleus (B). The third ventricle is marked (3 V). Body weight of male mice at 14 weeks of age (C). Whole body DXA data: Lean mass (D), fat mass (E) and % fat mass (F). Serum leptin levels as determined by ELISA (G). Dissected gonadal white adipose tissue weight (H) and expressed as % of body weight (I). Representative images of haematoxylin and eosin staining of gonadal white adipose tissue (J). Mean ± SEM. Statistical analysis: Students *t*-test (C–I), where $*p < .05$. Body weight and DXA analyses: Male WT ($n = 5$); Male NPYKO ($n = 7$).

Meulen et al., 2001); the computed indices of strength generated from the microCT data implied that male NPYKO bones would be weaker in terms of bending properties (Suppl. Table 1). Our torsion testing of WT and NPYKO femurs identified that NPYKO mice had weaker bones as they had an 18% reduction in bone strength in comparison to WT mice (Fig. 4J). No significant difference in bone stiffness was found between WT and NPYKO (Fig. 4K), suggesting that the reduction observed reduction in strength may be associated with the change in cross-sectional area. Altogether, this data shows that male NPYKO mice have a smaller cross-sectional area in comparison to WT mice and impaired bone strength.

Consistent with the reduction in cross-sectional bone area observed in the cortical region of interest (ROI), a reduction in total bone volume and tissue volume were observed in the cancellous ROI (Fig. 5A). However, the bone volume to tissue volume ratio (BV/TV) between WT and NPYKO mice was not significantly different (Fig. 5B). No significant differences in trabecular thickness and trabecular number were identified (Fig. 5C, D). Histomorphometric analysis of dynamic labeling in the cancellous region indicated that there was no change in mineral apposition rate, mineralizing surface or bone formation rate (Fig. 5E, F, G). NPY-deficiency did not affect osteoclast number or surface in NPYKO mice (Fig. 5H, I); consistent with our data showing that osteoclasts do not express the Y1 receptor (Fig. 2D). The effects of NPY deficiency primarily reduce bone length, cortical cross-sectional area and bone strength.

3.5. Sex-specific effects of NPY on the skeleton

Sexual dimorphism has been observed in metabolic studies with other NPY models (Karl et al., 2008; Zammaretti et al., 2007; Allison et al., 2009; Han et al., 2012). Therefore, we examined female mice of the same age to determine whether NPY-deficiency had the same effect in male and female mice. At 14 weeks of age, a significant increase in body weight was observed in female NPYKO mice in comparison to WT mice (Table 2). This increase in body weight was attributed to both an increase in lean mass and fat mass (Table 2). Thus, increased adiposity was observed in both sexes, however the metabolic effects of NPY-deficiency in female mice were greater in magnitude in comparison to male. Leptin levels were elevated in female NPYKO mice corresponding with increased fat mass (Table 2). Femoral length had a trend towards a reduction in female NPYKO mice (Table 2, $p = .14$), similar to the observation in male mice. However, no changes in bone cross-sectional area, cortical or cancellous bone mass were identified in female NPYKO mice (Table 2). The presence of changes in body composition similar to male NPYKO mice and the absence of a bone phenotype in female mice suggest that there may be sex-specific effects of NPY on the skeleton.

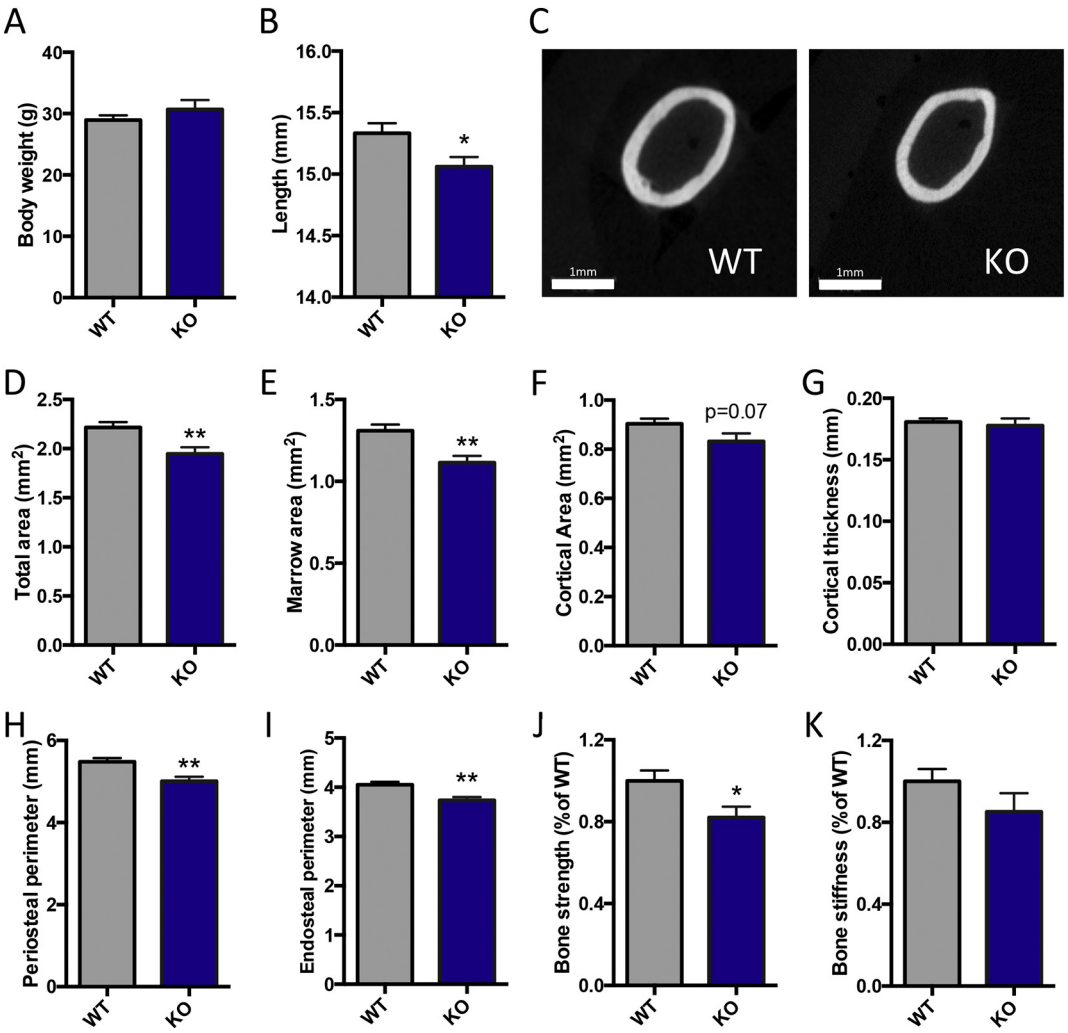

Fig. 4. ***Male NPYKO femurs have a smaller cortical cross-sectional area and reduced bone strength.*** Body weight (A) and femoral length (B) of mice at 14 weeks of age. Representative images of WT and NPYKO in mid-diaphyseal region of the femur (C). MicroCT analysis: total area (D), marrow area (E), cortical area (F), cortical thickness (G) periosteal perimeter (H) and endosteal perimeter (I). Torsion testing: bone strength (J) and bone stiffness (K). Mean ± SEM. Statistical analysis: Students t-test (A, B, D–J), where *p < .05 and **p < .01. Body weight, femoral length and microCT analyses: male WT (n = 14); male NPYKO (n = 13). Torsion testing: male WT (n = 8); male NPYKO (n = 8).

3.6. In vitro cultures of NPYKO BMSCs show increased osteoblastic differentiation

BMSCs were isolated from female WT and NPYKO mice (Fig. 6A). Increased alkaline phosphatase staining was observed in NPYKO cultures (Fig. 6B). In WT cultures, *Npy* expression decreased with differentiation at Day 14 and Day 21; and as expected, was absent in the NPYKO BMSCs (Fig. 6C). *Y1* receptor expression in WT BMSCs increased on days 14 and 21 following differentiation (Fig. 6D). *Y1* expression was unaltered during the differentiation of NPYKO BMSCs (Fig. 6D). As expected, bone sialoprotein (*Bsp*) and osteocalcin (*Ocn*) levels increased in WT mice with differentiation (Fig. 6E, F). In comparison, BMSCs from NPYKO mice had greater expression of *Bsp* and *Ocn* on day 14 and day 21 of culture, indicating that NPY-deficient BMSCs have enhanced differentiation (Fig. 6E, F). Cultures derived from male mice showed the same increase in ALP staining and increased mineralization (data not shown). These *in vitro* experiments are consistent with reports in other NPY models (Matic et al., 2012; Igwe et al., 2009; Baldock et al., 2007) and suggest that the skeletal phenotype observed in global NPY deficiency may be complex due to the role of NPY in multiple systems (*i.e.* central and peripheral nervous systems) and also its local production in bone.

4. Discussion

To better understand the sources of NPY and its receptors in bone tissues and bone derived cell cultures; we completed a comprehensive analysis of their expression. While we confirmed *Npy* expression in more mature osteoblast lineage cells, a high level of expression was detected in BMMs induced by RANKL. *Y1* receptor expression was detected in mature osteoblasts but not in BMMs, thus suggesting that BMMs may be a source of NPY but not respond to NPY stimulation. We have generated a novel murine model allowing for conditional deletion of NPY. By crossing our NPY floxed mice with *Hprt*-cre to generate a global knockout, we validated and confirmed loss of *Npy* transcript and protein in our global NPYKO. Male NPYKO mice had a smaller cross-section in the femur and reduced bone strength. *In vitro* NPY-deficient BMSCs showed enhanced differentiation. Altogether, this work confirms *Npy* expression in the skeleton and by generating a conditional knockout we have been able to establish a model to dissect the contribution of NPY from specific cell types.

The skeletal phenotype of reduced cortical cross section and impaired bone strength determined using our global NPYKO differs from other NPY-deficient models previously published. Elefteriou et al. (2003) examined the NPY deficient model (NPY^{tm1RPA}) on a 129SV/

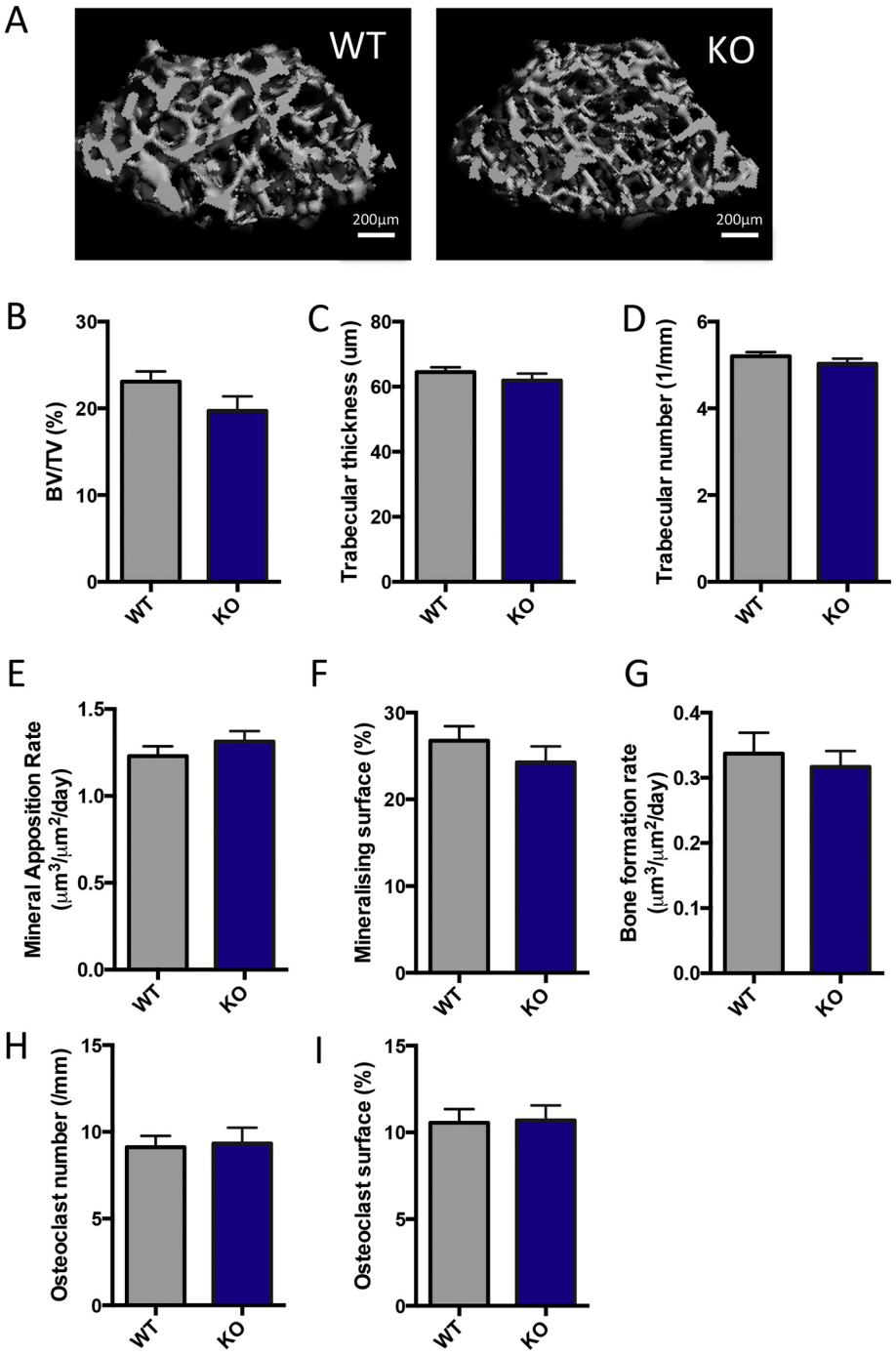

Fig. 5. NPY-deficiency does not affect cancellous bone. Representative images from male WT and NPYKO mice (A). MicroCT analysis: BV/TV (B), trabecular thickness (C) and trabecular number (D). Dynamic histomorphometry: mineral apposition rate (E), mineralizing surface (F), and bone formation rate (G). TRAP staining: osteoclast number (H) and osteoclast surface (I). Mean ± SEM. Statistical analysis: Students t-test (B–I). Male WT (n = 14); Male NPYKO (n = 13).

C57BL6 background whereby exon 2 of the *Npy* gene was replaced by a LacZ-neo fusion cassette. These mice had no differences in cancellous bone mass, but only vertebral bone mass was examined (Elefteriou et al., 2003). Wang et al. (2016) also utilized the NPY^{tm1RPA} mouse model on a 129SV background and reported significant increases in both femoral cortical and cancellous bone mass (Wang et al., 2016). The global NPYKO model ($Npy^{tm1(cre)Tkar}$) on a mixed 129SV/C57BL6 background has been frequently used in studies by Baldock et al. (Baldock et al., 2009, 2014; Wee et al., 2018; Wong et al., 2013); this model was generated by knocking-in a cre construct into exon 2 of the *Npy* locus, which resulted in a null allele (Karl et al., 2008). These studies demonstrated that NPY deficiency results in increased cortical bone mass. Effects on cancellous bone in this model are context-dependent. The construction of each of these global NPYKO mice has been different, and each involved insertion of genes into the locus (lacZ-neo cassette or cre-recombinase) which may affect the phenotype. Differing genetic backgrounds of the mice may also account for the differences in the effects on bone mass (Bouxsein et al., 2005; Turner et al., 2000; Li et al., 2005).

In addition, the complexity of the NPYKO model may be attributed to a combination of Y receptor deficiency phenotypes since we have removed the ligand from all tissues. The Y1 receptor knockout mouse

Table 2
Characteristics of female NPYKO mice (Mean ± SEM).

Measurement	WT n = 7	NPYKO n = 6
Metabolic		
Body weight (g)	**20.87 ± 0.18**	**26.22 ± 1.78****
Lean mass (g)	**15.23 ± 0.11**	**16.78 ± 0.61***
Fat mass (g)	**3.30 ± 0.18**	**7.18 ± 1.26****
% Fat mass	**17.7 ± 0.9**	**29.2 ± 3.0***
Leptin levels (ng/mL)	**2.26 ± 0.4**	**6.63 ± 1.7***
Bone		
Femur length	14.97 ± 0.08	14.75 ± 0.12
Total area (mm^2)	1.67 ± 0.02	1.66 ± 0.05
Marrow area (mm2)	0.98 ± 0.01	0.97 ± 0.04
Cortical area (mm2)	0.69 ± 0.01	0.69 ± 0.02
Cortical thickness (mm)	0.158 ± 0.003	0.161 ± 0.002
Periosteal perimeter (mm)	4.67 ± 0.04	4.65 ± 0.07
Endosteal perimeter (mm)	3.50 ± 0.03	3.48 ± 0.06
BV/TV (%)	4.8 ± 0.8	5.0 ± 0.8
Trabecular thickness (μm)	49.0 ± 1.1	48.3 ± 1.6
Trabecular number (1/mm)	3.3 ± 0.1	3.4 ± 0.1

*Student's t-test, *p < .05, **p < .01 when compared to WT.

displays a phenotype of adult-onset obesity and increases in cortical bone mass (Baldock et al., 2007). In addition to the significant increases in bone formation rate, global Y1 receptor knockout mice have increased osteoclast surface (Baldock et al., 2007). This has been recapitulated in peripheral Y1 antagonist BIBO3304-treated mice (Sousa et al., 2012). Recently, Sousa et al. (2016) suggested that osteoclasts from Y1 deficient mice have reduced ability to resorb bone, and thus, this coupled to increased bone formation, led to the observed phenotype of increased bone mass in Y1 deficient mice (Sousa et al., 2016). Mice with a specific deletion of the Y1 receptor from osteoblasts and osteocytes have no changes in adiposity and an increase in cortical bone mass (Lee et al., 2011). These mice have no changes in osteoclastic parameters suggesting that NPY signaling through the osteoblast is not influencing osteoclasts. Baldock et al. (2002) reported increases in cortical and cancellous bone mass in their Y2KO maintained on a mixed C57/Bl6-129Sv background (Baldock et al., 2002). However, Mikic et al. (2008) observed in their Y2KO on a mixed 129Sv-Balb/C background that these mice had smaller cortical cross-sections, less cortical bone area and lower structural strength (Mikic et al., 2008). Y6-deficient mice have reduced cortical and cancellous bone mass, which was associated with an increase in osteoclast progenitors leading to increased resorption and a decrease in osteoblast progenitors leading to reduced osteoblast activity (Khor et al., 2016). Altogether, the differences observed with each of these models demonstrate the complexity involved between NPY and its receptors and the impact that central signaling external to bone can have on the skeleton.

Both sexes had significant increases in adiposity; however, we only observed a bone phenotype in male NPYKO mice. Sexual dimorphism has been observed with other NPY models (Karl et al., 2008; Zammaretti et al., 2007; Allison et al., 2009; Han et al., 2012). While the majority of studies focusing on bone have reported the same phenotype between both sexes (Baldock et al., 2007, 2009; Khor et al., 2016), there has been evidence that NPY-Y1 signaling increases bone mass in the presence of androgens as no differences in bone mass were found between WT and Y1KO mice that had undergone gonadectomy (Allison et al., 2009). Estrogen is known to affect bone remodeling (Khosla et al., 2012) and estrogen deficiency increases sympathetic activity (Gomes et al., 2012). Since NPY can inhibit sympathetic activity, this may have subsequent effects on bone. A metabolic study has shown that NPY ablated the reduction in energy expenditure and increase in fat mass induced by short-term estrogen deficiency (Zengin et al., 2013). These studies suggest that androgens and estrogen may be factors involved in understanding the sex-specific skeletal differences we observed.

Npy is expressed in the nervous system and also in the periphery. Here, we have observed *Npy* expression in bone and primary cells (BMMs, BMSCs and calvarial osteoblasts). While local overexpression of NPY in osteoblasts using the *Col1a1* 2.3 kb reporter reduces cortical bone mass (Matic et al., 2012), there has not been any assessment of local endogenous NPY production. By generating the conditional NPY mouse, we will be able to explore the effect of local NPY deficiency by targeting different cell types using specific cre models. The targeted nature of these future models will assist in separating the multitude of effects observed in our global NPYKO. It is likely that some of the phenotype (*i.e.* adiposity) observed in the NPYKO is attributed to changes in central NPY signaling. The observed effect on bone mass in our NPYKO model may be arising from direct loss of NPY signaling, or through indirect effects such as the influence of adipose tissue on bone. Increased adiposity can lead to increases in cortical bone mass due to the positive effects of load bearing, but at the same time increases in sympathetic tone, inflammatory cytokines and oxidative stress which can negatively impact bone mass (Wee et al., 2018; Cao, 2011; Cao and Picklo, 2014). The effects of other tissues on bone mass may explain the difference we observed between our *in vivo* and *in vitro* studies. While bone mass was impacted by global NPY deficiency, further work is required to dissect and determine the contribution of individual NPY sources.

There are a few limitations of this study. The skeleton is constantly being remodeled. During development there is rapid growth and modeling occurring, followed by the attainment of peak bone mass and further remodeling. We examined the effect of NPY deficiency at a single time point that represents adult animals nearing peak bone mass. It is possible that examining mice at different ages may help to elucidate the role of NPY during different stages of bone modeling and remodeling. While our focus was on the skeletal phenotype of these mice, our analysis of the changes in fat mass were limited and had a small n. It is difficult to gauge why these NPYKO mice have increased adiposity from these observations, thus further examination of the metabolic phenotype (such as food intake, energy expenditure, *etc.*) is needed to elucidate the mechanisms involved.

We have developed the NPY conditional mouse and generated a global NPY deficient model to examine the impact of NPY signaling on bone. Our study has identified that global NPY deficiency regulates bone mass and in this case, leads to smaller bones with impaired strength. Notably, the findings of this study clearly demonstrate that global deficiency contributes to the overall phenotype through various mechanisms and this may explain the discrepancy we observed between our *in vivo* and *ex vivo* results. Since *Npy* is expressed in both the nervous system and skeletal tissues and influences energy metabolism, our work in this study generating and characterizing the NPY floxed mouse will facilitate the selective depletion of NPY from different cell populations *in vivo* to dissect the contribution of central and local NPY signaling in the future.

Supplementary data to this article can be found online at https://doi.org/10.1016/j.npep.2018.11.009.

Disclosures

All authors have no conflicts of interest regarding this manuscript.

Acknowledgements

We would like to thank Dr. Sun-Kyeong Lee (UConn Health) for provision of cDNA to assess NPY and Y1 levels in BMMs in response to RANKL stimulation. We would also like to thank Dr. Mark Kronenberg (UConn Health) for provision of RNA from calvarial osteoblast culture time courses. This work has been supported by NIH/NIAMS grants AR055607, AR066218, Connecticut Innovations (CI) 16-RMB-UCHC-10 and REP funds to IK, and Health Research Council of New Zealand Sir Charles Hercus Fellowship to BGM.

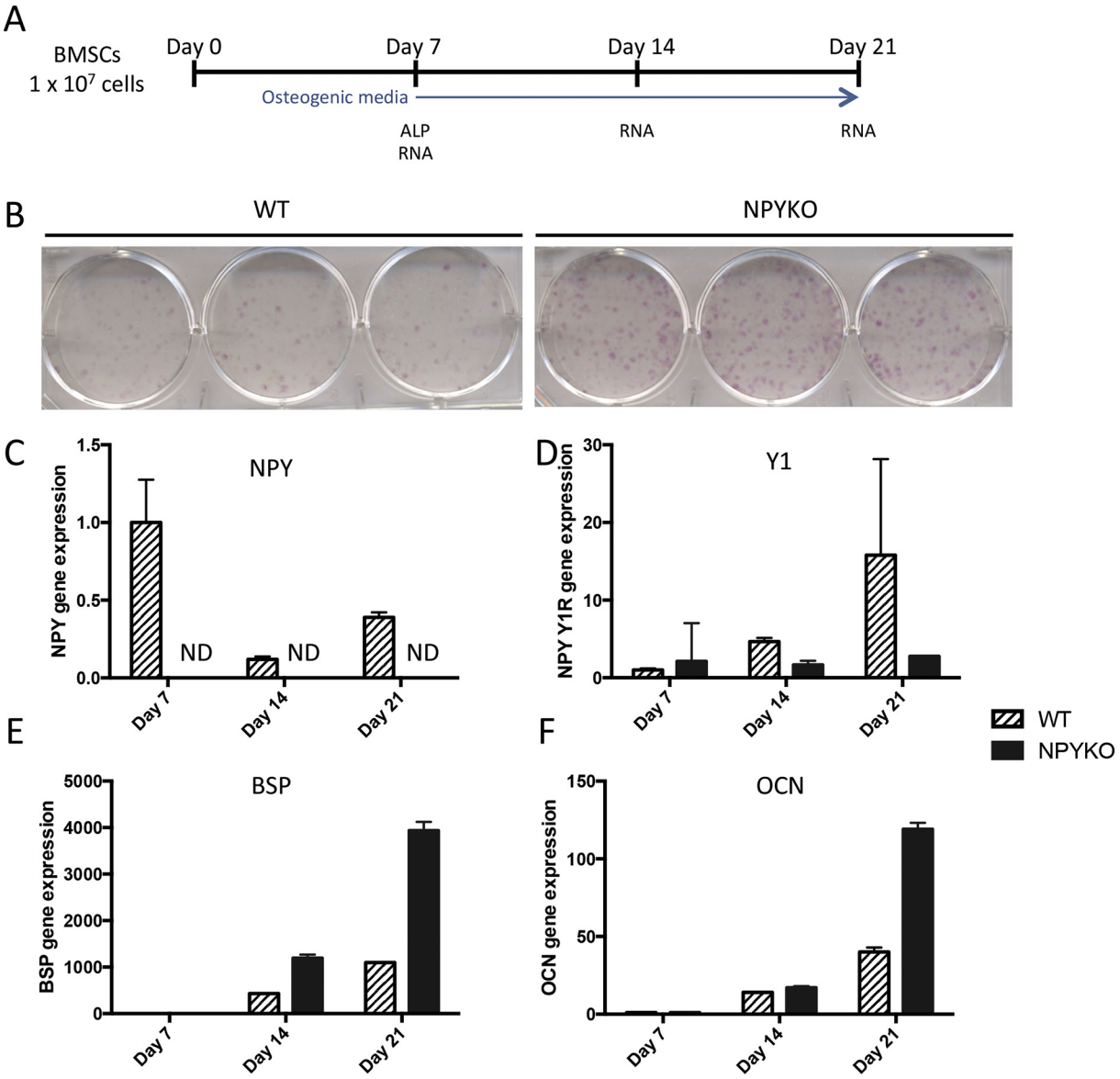

Fig. 6. ***BMSC cultures from NPYKO mice in osteogenic media have increased differentiation.*** Schematic diagram of BMSC culture and time points (A). Alkaline phosphatase staining of Day 7 BMSCs (B); one representative experiment is shown, from $n = 4$ independent biological replicates. Time course of gene expression of neuropeptide Y (C), Y1 receptor (D), bone sialoprotein (E) and osteocalcin (F). Expression was not detectable (ND) by qPCR. One representative experiment is shown, n = 2 independent biological experiments.

References

Allison, S.J., Baldock, P.A., Enriquez, R.F., Lin, E., During, M., Gardiner, E.M., Eisman, J.A., Sainsbury, A., Herzog, H., 2009. Critical interplay between neuropeptide Y and sex steroid pathways in bone and adipose tissue homeostasis. J. Bone Miner. Res. 24, 294–304.

Alves, C.J., Alencastre, I.S., Neto, E., Ribas, J., Ferreira, S., Vasconcelos, D.M., Sousa, D.M., Summavielle, T., Lamghari, M., 2016. Bone injury and repair trigger central and peripheral NPY neuronal pathways. PLoS One 11, e0165465.

Baldock, P.A., Sainsbury, A., Couzens, M., Enriquez, R.F., Thomas, G.P., Gardiner, E.M., Herzog, H., 2002. Hypothalamic Y2 receptors regulate bone formation. J. Clin. Invest. 109, 915–921.

Baldock, P.A., Allison, S.J., Lundberg, P., Lee, N.J., Slack, K., Lin, E.J., Enriquez, R.F., McDonald, M.M., Zhang, L., During, M.J., Little, D.G., Eisman, J.A., Gardiner, E.M., Yulyaningsih, E., Lin, S., Sainsbury, A., Herzog, H., 2007. Novel role of Y1 receptors in the coordinated regulation of bone and energy homeostasis. J. Biol. Chem. 282, 19092–19102.

Baldock, P.A., Lee, N.J., Driessler, F., Lin, S., Allison, S., Stehrer, B., Lin, E.J., Zhang, L., Enriquez, R.F., Wong, I.P., McDonald, M.M., During, M., Pierroz, D.D., Slack, K., Shi, Y.C., Yulyaningsih, E., Aljanova, A., Little, D.G., Ferrari, S.L., Sainsbury, A., Eisman, J.A., Herzog, H., 2009. Neuropeptide Y knockout mice reveal a central role of NPY in the coordination of bone mass to body weight. PLoS One 4, e8415.

Baldock, P.A., Lin, S., Zhang, L., Karl, T., Shi, Y., Driessler, F., Zengin, A., Hormer, B., Lee, N.J., Wong, I.P., Lin, E.J., Enriquez, R.F., Stehrer, B., During, M.J., Yulyaningsih, E., Zolotukhin, S., Ruohonen, S.T., Savontaus, E., Sainsbury, A., Herzog, H., 2014. Neuropeptide y attenuates stress-induced bone loss through suppression of noradrenaline circuits. J. Bone Miner. Res. 29, 2238–2249.

Blomqvist, A.G., Herzog, H., 1997. Y-receptor subtypes–how many more? Trends Neurosci. 20, 294–298.

Bouxsein, M.L., Myers, K.S., Shultz, K.L., Donahue, L.R., Rosen, C.J., Beamer, W.G., 2005. Ovariectomy-induced bone loss varies among inbred strains of mice. J. Bone Miner. Res. 20, 1085–1092.

Cao, J.J., 2011. Effects of obesity on bone metabolism. J. Orthop. Surg. Res. 6, 30.

Cao, J.J., Picklo, M.J., 2014. N-acetylcysteine supplementation decreases osteoclast differentiation and increases bone mass in mice fed a high-fat diet. J. Nutr. 144, 289–296.

Chang, M.K., Raggatt, L.J., Alexander, K.A., Kuliwaba, J.S., Fazzalari, N.L., Schroder, K., Maylin, E.R., Ripoll, V.M., Hume, D.A., Pettit, A.R., 2008. Osteal tissue macrophages are intercalated throughout human and mouse bone lining tissues and regulate osteoblast function in vitro and in vivo. J. Immunol. 181, 1232–1244.

Dempster, D.W., Compston, J.E., Drezner, M.K., Glorieux, F.H., Kanis, J.A., Malluche, H., Meunier, P.J., Ott, S.M., Recker, R.R., Parfitt, A.M., 2013. Standardized nomenclature, symbols, and units for bone histomorphometry: a 2012 update of the report of the ASBMR Histomorphometry Nomenclature Committee. J. Bone Miner. Res. 28, 2–17.

van der Meulen, M.C., Jepsen, K.J., Mikic, B., 2001. Understanding bone strength: size isn't everything. Bone 29, 101–104.

Ducy, P., Amling, M., Takeda, S., Priemel, M., Schilling, A.F., Beil, F.T., Shen, J., Vinson, C., Rueger, J.M., Karsenty, G., 2000. Leptin inhibits bone formation through a hypothalamic relay: a central control of bone mass. Cell 100, 197–207.
Elefteriou, F., Takeda, S., Liu, X., Armstrong, D., Karsenty, G., 2003. Monosodium glutamate-sensitive hypothalamic neurons contribute to the control of bone mass. Endocrinology 144, 3842–3847.
Gomes, H.L., Graceli, J.B., Goncalves, W.L., dos Santos, R.L., Abreu, G.R., Bissoli, N.S., Pires, J.G., Cicilini, M.A., Moyses, M.R., 2012. Influence of gender and estrous cycle on plasma and renal catecholamine levels in rats. Can. J. Physiol. Pharmacol. 90, 75–82.
Han, R., Li, A., Li, L., Kitlinska, J.B., Zukowska, Z., 2012. Maternal low-protein diet upregulates the neuropeptide Y system in visceral fat and leads to abdominal obesity and glucose intolerance in a sex- and time-specific manner. FASEB J. 26, 3528–3536.
Horsnell, H., Baldock, P.A., 2016. Osteoblastic actions of the neuropeptide Y system to regulate bone and energy homeostasis. Curr. Osteoporos Rep. 14, 26–31.
Igwe, J.C., Jiang, X., Paic, F., Ma, L., Adams, D.J., Baldock, P.A., Pilbeam, C.C., Kalajzic, I., 2009. Neuropeptide Y is expressed by osteocytes and can inhibit osteoblastic activity. J. Cell. Biochem. 108, 621–630.
Karl, T., Duffy, L., Herzog, H., 2008. Behavioural profile of a new mouse model for NPY deficiency. Eur. J. Neurosci. 28, 173–180.
Khor, E.C., Yulyaningsih, E., Driessler, F., Kovacic, N., Wee, N.K.Y., Kulkarni, R.N., Lee, N.J., Enriquez, R.F., Xu, J., Zhang, L., Herzog, H., Baldock, P.A., 2016. The y6 receptor suppresses bone resorption and stimulates bone formation in mice via a suprachiasmatic nucleus relay. Bone 84, 139–147.
Khosla, S., Oursler, M.J., Monroe, D.G., 2012. Estrogen and the skeleton. Trends Endocrinol. Metab. 23, 576–581.
Lee, N.J., Doyle, K.L., Sainsbury, A., Enriquez, R.F., Hort, Y.J., Riepler, S.J., Baldock, P.A., Herzog, H., 2010. Critical role for Y1 receptors in mesenchymal progenitor cell differentiation and osteoblast activity. J. Bone Miner. Res. 25, 1736–1747.
Lee, N.J., Nguyen, A.D., Enriquez, R.F., Doyle, K.L., Sainsbury, A., Baldock, P.A., Herzog, H., 2011. Osteoblast specific Y1 receptor deletion enhances bone mass. Bone 48, 461–467.
Lee, N.J., Nguyen, A.D., Enriquez, R.F., Luzuriaga, J., Bensellam, M., Laybutt, R., Baldock, P.A., Herzog, H., 2015. NPY signalling in early osteoblasts controls glucose homeostasis. Mol. Metab. 4, 164–174.
Li, C.Y., Schaffler, M.B., Wolde-Semait, H.T., Hernandez, C.J., Jepsen, K.J., 2005. Genetic background influences cortical bone response to ovariectomy. J. Bone Miner. Res. 20, 2150–2158.
Matic, I., Matthews, B.G., Kizivat, T., Igwe, J.C., Marijanovic, I., Ruohonen, S.T., Savontaus, E., Adams, D.J., Kalajzic, I., 2012. Bone-specific overexpression of NPY modulates osteogenesis. J. Musculoskelet. Neuronal Interact. 12, 209–218.
Mikic, B., Zhang, M., Webster, E., Rossmeier, K., 2008. Effect of y2 receptor deletion on whole bone structural behavior in mice. Anat. Rec. (Hoboken) 291, 14–18.
Paic, F., Igwe, J.C., Nori, R., Kronenberg, M.S., Franceschetti, T., Harrington, P., Kuo, L., Shin, D.G., Rowe, D.W., Harris, S.E., Kalajzic, I., 2009. Identification of differentially expressed genes between osteoblasts and osteocytes. Bone 45, 682–692.
Park, M.H., Lee, J.K., Kim, N., Min, W.K., Lee, J.E., Kim, K.T., Akiyama, H., Herzog, H., Schuchman, E.H., Jin, H.K., Bae, J.S., 2016. Neuropeptide Y induces hematopoietic stem/progenitor cell mobilization by regulating matrix metalloproteinase-9 activity through Y1 receptor in osteoblasts. Stem Cells 34, 2145–2156.
Schwartz, T.W., Fuhlendorff, J., Kjems, L.L., Kristensen, M.S., Vervelde, M., O'Hare, M., Krstenansky, J.L., Bjornholm, B., 1990. Signal epitopes in the three-dimensional structure of neuropeptide Y. Interaction with Y1, Y2, and pancreatic polypeptide receptors. Ann. N. Y. Acad. Sci. 611, 35–47.
Sousa, D.M., Baldock, P.A., Enriquez, R.F., Zhang, L., Sainsbury, A., Lamghari, M., Herzog, H., 2012. Neuropeptide Y Y1 receptor antagonism increases bone mass in mice. Bone 51, 8–16.
Sousa, D.M., Conceicao, F., Silva, D.I., Leitao, L., Neto, E., Alves, C.J., Alencastre, I.S., Herzog, H., Aguiar, P., Lamghari, M., 2016. Ablation of Y1 receptor impairs osteoclast bone-resorbing activity. Sci. Rep. 6, 33470.
Tabarowski, Z., Gibson-Berry, K., Felten, S.Y., 1996. Noradrenergic and peptidergic innervation of the mouse femur bone marrow. Acta Histochem. 98, 453–457.
Turner, C.H., Hsieh, Y.F., Muller, R., Bouxsein, M.L., Baylink, D.J., Rosen, C.J., Grynpas, M.D., Donahue, L.R., Beamer, W.G., 2000. Genetic regulation of cortical and trabecular bone strength and microstructure in inbred strains of mice. J. Bone Miner. Res. 15, 1126–1131.
Wang, F.S., Lian, W.S., Weng, W.T., Sun, Y.C., Ke, H.J., Chen, Y.S., Ko, J.Y., 2016. Neuropeptide Y mediates glucocorticoid-induced osteoporosis and marrow adiposity in mice. Osteoporos. Int. 27, 2777–2789.
Wee, N.K., Kulkarni, R.N., Horsnell, H., Baldock, P.A., 2016. The brain in bone and fuel metabolism. Bone 82, 56–63.
Wee, N.K.Y., Enriquez, R.F., Nguyen, A.D., Horsnell, H., Kulkarni, R., Khor, E.C., Herzog, H., Baldock, P.A., 2018. Diet-induced obesity suppresses cortical bone accrual by a neuropeptide Y-dependent mechanism. Int. J. Obes. 42 (11), 1925–1938.
Wheway, J., Herzog, H., Mackay, F., 2007. The Y1 receptor for NPY: a key modulator of the adaptive immune system. Peptides 28, 453–458.
Wong, I.P., Nguyen, A.D., Khor, E.C., Enriquez, R.F., Eisman, J.A., Sainsbury, A., Herzog, H., Baldock, P.A., 2013. Neuropeptide Y is a critical modulator of leptin's regulation of cortical bone. J. Bone Miner. Res. 28, 886–898.
Yeon Won, H., Hwan Mun, S., Shin, B., Lee, S.K., 2016. Contradictory role of CD97 in basal and tumor necrosis factor-induced osteoclastogenesis in vivo. Arthritis Rheumatol. 68, 1301–1313.
Zammaretti, F., Panzica, G., Eva, C., 2007. Sex-dependent regulation of hypothalamic neuropeptide Y-Y1 receptor gene expression in moderate/high fat, high-energy diet-fed mice. J. Physiol. 583, 445–454.
Zengin, A., Nguyen, A.D., Wong, I.P., Zhang, L., Enriquez, R.F., Eisman, J.A., Herzog, H., Baldock, P.A., Sainsbury, A., 2013. Neuropeptide Y mediates the short-term hypometabolic effect of estrogen deficiency in mice. Int. J. Obes. 37, 390–398.
Zhang, L., Macia, L., Turner, N., Enriquez, R.F., Riepler, S.J., Nguyen, A.D., Lin, S., Lee, N.J., Shi, Y.C., Yulyaningsih, E., Slack, K., Baldock, P.A., Herzog, H., Sainsbury, A., 2010. Peripheral neuropeptide Y Y1 receptors regulate lipid oxidation and fat accretion. Int. J. Obes. 34, 357–373.